Effect of reduction on the molecular structure, optical and magnetic properties of the fluorinated copper (II) phthalocyanines

ROYAL SOCIETY
OF CHEMISTRY

Journal Name

ARTICLE

Effect of reduction on the molecular structure, optical and magnetic properties of the fluorinated copper (II) phthalocyanines†

Dmitri V. Konarev,*[a] Maxim A. Faraonov, *[a] Mikhail S. Batov, [a,b] Mikhail G. Andronov, [a,b]

Alexey V. Kuzmin,[c] Salavat S. Khasanov, [c] Akihiro Otsuka,[d, e] Hideki Yamochi,[d, e] Hiroshi Kitagawa[d]

Rimma N. Lyubovskaya[a]

Reduction of copper(II) octafluoro- $\{Cu^{II}(F_8Pc)\}$ and hexadecafluorophthalocyanines $\{Cu^{II}(F_{16}Pc)\}$ by $NaCpCo(CO)_2$ in the presence of cryptand[2.2.2] yields new crystalline $\{cryptand(Na^+)\}[Cu^{II}(F_8Pc)^{\bullet 3-}]^-\cdot 2C_6H_4Cl_2$ (**1**) and $\{cryptand(Na^+)\}_2[Cu^{II}(F_{16}Pc)^{4-}]^{2-}\cdot C_6H_{14}$ (**2**) salts. Together with two previously characterized salts of $Cu^{II}(F_xPc)$ (x = 8 and 16), this allows the study of the molecular structure, optical and magnetic properties of fluorinated copper phthalocyanines in different reduction states (-1 and -2). Blue shift of the Q-band increases together with negative charge on the macrocycle, and new weak bands of the anions appear at 820-1013 nm. Alternation of the N_{meso}-C bonds manifests itself in reduced macrocycles due to partial disruption of macrocycle aromaticity. In case of $Cu^{II}(F_8Pc)$ this effect is nearly two times stronger for the dianions than for monoanions. Alternation of bonds is less pronounced for perfluorinated $Cu^{II}(F_{16}Pc)^{n-}$ (n = 1, 2) anions most probably due to partial delocalization of negative charge on fluoro-substituents. Reduction also noticeably elongates average C-F bonds in $Cu^{II}(F_8Pc)$. First reduction centered on the macrocycle provides the formation of $[Cu^{II}(F_8Pc)^{\bullet 3-}]^-$ in **1** with two S = 1/2 spins positioned on Cu^{II} and radical trianion $(F_8Pc)^{\bullet 3-}$ macrocycle. As a result, a broad EPR signal is observed with g = 2.1652 at RT attributable to both paramagnetic species having exchange interactions. The formation of dimerized stacks from $[Cu^{II}(F_8Pc)^{\bullet 3-}]^-$ in **1** results in strong enough magnetic coupling of the $(F_8Pc)^{\bullet 3-}$ spins within the dimers (J/k_B = - 21.8 cm^{-1}), and weaker intramolecular coupling is observed between Cu^{II} and $(F_8Pc)^{\bullet 3-}$ (J/k_B = -10.8 cm^{-1}). Coupling between $(F_8Pc)^{\bullet 3-}$ spins from the neighboring dimers is nearly 1.5 times weaker (-14.6 cm^{-1}). In reduction conditions a second electron also comes to the macrocycle forming diamagnetic $F_{16}Pc^{4-}$ tetraanions. In this case S =1/2 spin is preserved on Cu^{II}. Magnetic coupling between these centers is weak due to long distances between them in the $[Cu^{II}(F_8Pc)^{4-}]^{2-}$ chains of **2**. Salt **2** manifests an EPR signal with HF splitting characteristic of Cu^{II} with $g_{||}$ = 2.1806 ($A_{||}$ = 20.11 mT), and $g_\perp$ = 1.9597 at RT.

Introduction

Metal phthalocyanines (MPcs) are a family of stable and cost-effective organic semiconductors of *p*- and *n*-types [1–3].

[a]Institute of Problems of Chemical Physics RAS, Chernogolovka, Moscow region, 142432 Russia; E-mails: konarev3@yandex.ru; maksimfaraonov@yandex.ru
[b]Moscow State University, Leninskie Gory,119991 Moscow, Russia;
[c]Institute of Solid State Physics RAS, Chernogolovka, Moscow region, 142432 Russia;
[d]Division of Chemistry, Graduate School of Science, Kyoto University, Sakyo-ku, Kyoto 606- 8502, Japan;
[e]Research Center for Low Temperature and Materials Sciences, Kyoto University, Sakyo-ku, Kyoto 606-8501, Japan.

Introduction of strong electron-withdrawing groups to the Pc macrocycle provides the possibility of changing their transport behavior [2,4]. Conducting properties of Pcs can successfully be modified by fluorination of the macrocycle [4–6] making fluorinated metal phthalocyanines promising components of organic optoelectronics devices [4]. Injection of additional electrons into phthalocyanines and related compounds upon reduction gives an extra opportunity to tune properties of Pc-based materials [7–10]. Acceptance of additional electrons by the macrocycles under reduction provides new properties since unpaired spin can participate in magnetic coupling of spins or high conductivity. Metallomacrocycles with paramagnetic central metal atoms are of special interest since spin localized on metals can interact with electrons delocalized over the macrocycles. Thus, giant

magnetoresistance is observed for oxidized Fe^{III} containing phthalocyanines [11] or some effect on magnetic properties of the salts is observed at transition from titanyl phthalocyanine with diamagnetic Ti^{IV} (S = 0) to vanadyl phthalocyanine with paramagnetic V^{IV} (S = 1/2) [7].

Fluoro substituted copper(II) phthalocyanines are metallomacrocycles of another type with paramagnetic central Cu(II) atoms (S = 1/2). Electron accepting fluorine substitution increases essentially acceptor ability of these metallomacrocycles. For example, $Cu^{II}(F_{16}Pc)$ is reduced even at -0.21 and -0.90 V vs Ag/AgCl [12]. These potentials are up to 0.6 V more positive than those of pristine $Cu^{II}Pc$ (first and second reductions are at -0.84 and − 1.18 V vs SCE) [13]. The Cu(F_xPc) monoanions can be more air-stable in comparison with those of unsubstituted $Cu^{II}Pc$ which are extremely air-sensitive [14]. Macrocycles with chloro or fluoro substituents also tend to pack in π-stacks [15–17]. Such packing is more suitable for improving conductivity or effective magnetic interactions. Moreover, reduction of fluorinated Cu($F_{16}Pc$) can be centered not only on the macrocycles but metal centered reduction is also possible. In this case variation of properties of the obtained salts can be observed [15].

Previously we obtained and structurally characterized two salts of both copper(II) octafluoro- and hexadecafluorophthalocyanines (Table 1) [15]. In this work we use strong organometallic reductant $NaCpCo(CO)_2$ to incorporate sodium including cryptand[2.2.2] (abbreviated as cryptand). This allows one to increase essentially solubility of the obtained anions and prepare good quality single crystals of {cryptand(Na^+)}[$Cu^{II}(F_8Pc)^{\bullet 3-}$]$^-$·$2C_6H_4Cl_2$ (**1**) and {cryptand(Na^+)}$_2$[$Cu^{II}(F_{16}Pc)^{4-}$]$^{2-}$·C_6H_{14} (**2**) containing radical trianion and tetraanion macrocycles, respectively. Since previously obtained salts showed charge of the macrocycles different from those in **1** and **2** [15], the whole series of the reduction states (-1 and -2) is available now for both fluorinated copper (II) phthalocyanines. That allows one to study the effect of reduction on molecular structure, optical and magnetic properties of the fluorinated copper(II) phthalocyanines. Such effects are found in optical properties as well as geometry of the macrocycles. Reduction is mainly centered on the macrocycles yielding trianion and tetraanion Cu(F_xPc) macrocycles with different magnetic behavior observed in the π-stacks or layers from the metallomacrocycles.

Table 1. Composition of salts **1 – 4**.

N	Composition	Charge state of $Cu^{II}(F_xPc)$	Reference
1	{cryptand(Na^+)}[$Cu^{II}(F_8Pc)^{\bullet 3-}$]$^-$ ·$2C_6H_4Cl_2$	-1	this work
2	{cryptand(Na^+)}$_2$[$Cu^{II}(F_{16}Pc)^{4-}$]$^{2-}$·C_6H_{14}	-2	this work
3	{Bu_4N^+}$_2$[$Cu^{II}(F_8Pc)^{4-}$]$^{2-}$ $2C_6H_4Cl_2$	-2	[15]
4	(PPN^+)$_3$[$Cu(F_{16}Pc)$]$_3^{3-}$·$2C_6H_5CN$	-1	[15]
cryptand is 4,7,13,16,21,24-hexaoxa-1,10-diazabicyclo[8.8.8]hexacosane PPN^+ is bis(triphenylphosphoranylidene)ammonium			

Results and discussion

a. Synthesis

According to the redox potentials, such strong reductants as sodium fluorenone ketyl (E_{redox} = - 1.30 V vs SCE [18]) and sodium cyclopentadienyl cobalt dicarbonyl ($Na^+[CpCo(CO)_2]^-$, E_{redox} = - 1.85 V vs SCE [19]) are suitable for preparation of anionic salts of $Cu^{II}(F_xPc)$ (x = 8, 16).

Previously studied reduction of fluorinated copper(II) phthalocyanines shows that their anions are very weakly soluble in o-dichlorobenzene especially in case of $Cu^{II}(F_{16}Pc)$, and significant amount of more polar benzonitrile should be added for their dissolution [15]. In this work we use organometallic reductant $NaCpCoCO_2$ together with cryptand[2.2.2] in pure o-dichlorobenzene. Cryptand[2.2.2] provides dissolution of reductant in non-coordinated o-dichlorobenzene by forming the cryptand(Na^+) cations which also provide good solubility of obtained salts in o-dichlorobenzene in contrast to previously used Bu_4N^+ and PPN^+ cations. Dissolved amount of $NaCpCoCO_2$ is defined by the amount of cryptand[2.2.2]. In spite of that two equivalents of cryptand are used upon the reduction of both $Cu^{II}(F_8Pc)$ and $Cu^{II}(F_{16}Pc)$, the dianion salt is formed for $Cu^{II}(F_{16}Pc)$ and only monoanion salt is formed for $Cu^{II}(F_8Pc)$. That can be explained by stronger acceptor properties of $Cu^{II}(F_{16}Pc)$ as well as packing factors for these salts.

The salts were isolated from o-dichlorobenzene solutions as black prisms with copper luster characteristic of reduced metal phthalocyanines. For {cryptand(Na^+)}{$Cu^{II}(F_8Pc)^{\bullet 3-}$]$^-$·$2C_6H_4Cl_2$ (**1**) and {cryptand(Na^+)}$_2$[$Cu^{II}(F_{16}Pc)^{4-}$]$^{2-}$·C_6H_{14} (**2**) their compositions were determined from X-ray diffraction on single crystals. Several crystals tested from each synthesis showed the same unit cell parameters indicating the formation of only one crystal phase in each synthesis.

b. Optical properties

IR spectra of pristine compounds and salts **1-2** measured in KBr pellets are shown in Figs. S1, and the positions of the absorption bands are listed in Tables S1-S2. It is seen that IR spectra of **1** and **2** are superpositions of the absorption bands of starting phthalocyanines and cryptand with the shift of some absorption bands up to 9 cm^{-1} (Table S1). Largest shifts are observed for the intense bands at 1472 and 1490 cm^{-1} attributed to the C-F vibrations which are shifted to 1461 and 1481 cm^{-1} in the spectra of salts **1** and **2**, respectively.

The UV-visible-NIR spectra of parent phthalocyanines and salts **1–4** in KBr pellets are shown in Fig.1 and the positions of the absorption bands are listed in Table 2. Optical spectra of starting $Cu^{II}(F_8Pc)$ and $Cu^{II}(F_{16}Pc)$ are similar. They contain single Soret and split Q-bands as well as very weak absorption bands in the NIR range.
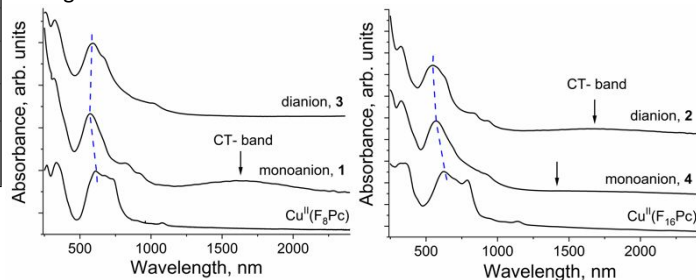

Fig. 1   UV-visible-NIR spectra for starting fluorinated phthalocyanines and salts **1 - 4** in KBr pellets in anaerobic conditions. Charge transfer bands are shown by arrows.

Table 2. Data of UV-visible-NIR spectra for starting phthalocyanines and salts **1** - **4**
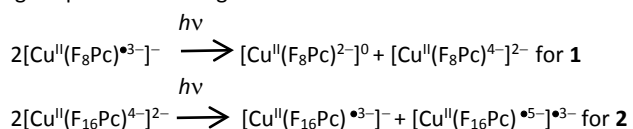
Compound	Charge state	Position of the absorption bands		
		Soret band, nm	Q-band, nm	Bands in NIR, nm
$Cu^{II}(F_8Pc)$	0	332	612 (max), 682, 735	1080
{cryptand(Na$^+$)}[Cu$^{II}(F_8Pc)^{3\bullet}$]$^-$ (**1**)	−1	317	574	821, 923, 1625 (CTB)
{Bu$_4$N$^+$}$_2$[Cu$^{II}(F_8Pc)^{4-}$]$^{2-}$·2C$_6$H$_4$Cl$_2$ (**3**) [15]	−2	319	590	1013
$Cu^{II}(F_{16}Pc)$	0	339	628 (max), 789	1137
(PPN$^+$)$_3$[Cu(F$_{16}$Pc)]$_3$$^{3-}$·2C$_6H_5$CN (**4**) [15]	−1	324	571	912, 1414 (CTB)
{cryptand(Na$^+$)}$_2$[Cu$^{II}(F_{16}Pc)^{4-}$]$^{2-}$ (**2**)	−2	324	544 (max), 623 (sh)	833, 934, 1670 (CTB)

Formation of **1**-**4** is accompanied by essential blue shift of the Q-bands in the spectra of the salts in comparison with the spectra of neutral metal phthalocyanines. Shift of the Q-band maximum at the reduction is essentially larger for $Cu^{II}(F_{16}Pc)$ than for $Cu^{II}(F_8Pc)$. These shifts are 38 are 22 nm for $(F_8Pc)^{\bullet 3-}$ and $(F_8Pc)^{4-}$ in **1** and **3**, respectively, whereas the shifts are 57 and 84 nm for $(F_{16}Pc)^{\bullet 3-}$ and $(F_{16}Pc)^{4-}$ in **4** and **2**, respectively. Previously, it was also shown that generally blue shift of the Q-bands increases together with negative charge on the phthalocyanine [20] or tetrapyrazinoporphirazine [10] macrocycles.

Both mono- and dianions show additional weak bands in the spectra of **1** − **4** in the NIR range at 820-920 nm (Fig. 1). These bands can appear at the LUMO population under reduction and the appearance of new transitions from this partially occupied LUMO to the above located orbitals. These new absorption bands in the NIR range are characteristic of all reduced phthalocyanine [20] and tetrapyrazinoporphirazine [21] macrocycles but it should be noted that generally these bands have essentially higher intensity in comparison with those in the spectra of **1**-**4**. Thus, weak absorption in the NIR range is characteristic of mono- and dianions of fluoro substituted phthalocyanine macrocycles only.

Broad absorption bands are observed in spectra of **1** and **2** with the maximum at 1625 and 1670 nm, respectively (Fig. 1). These bands can be attributed to charge transfer (CT) between copper(II) phthalocyanine anions observed in the stacks or chains of **1** and **2** at the absorption of light quantum. A similar CT band was found previously in the spectrum of **4** due to stacking arrangement of the macrocycles. Since intensity of these bands depends on the overlapping of π-orbitals of the macrocycles[7], such band is not found in the spectrum of **3** (Fig. 1) due to isolation of the [Cu$^{II}(F_8Pc)^{4-}$] dianions in this salt [15].

Electronic transfer between [Cu$^{II}(F_8Pc)^{3\bullet}$]$^-$ in the stacks of **1** or between [Cu$^{II}(F_{16}Pc)^{4-}$] in the layers of **2** produces differently charged species according to reactions:

$$2[Cu^{II}(F_8Pc)^{\bullet 3-}]^- \xrightarrow{h\nu} [Cu^{II}(F_8Pc)^{2-}]^0 + [Cu^{II}(F_8Pc)^{4-}]^{2-} \text{ for } \mathbf{1}$$

$$2[Cu^{II}(F_{16}Pc)^{4-}]^{2-} \xrightarrow{h\nu} [Cu^{II}(F_{16}Pc)^{\bullet 3-}]^- + [Cu^{II}(F_{16}Pc)^{\bullet 5-}]^{\bullet 3-} \text{ for } \mathbf{2}$$

Intensity of absorption CT bands depends on the overlapping of π-orbitals of macrocycles.

c. Crystal structure

Crystal structure of **1** contains one independent $Cu^{II}(F_8Pc)$ unit and a cryptand(Na$^+$) cation. There are half independent $Cu^{II}(F_{16}Pc)$ unit

and whole cryptand(Na$^+$) cation in **2**. According to the crystal structure data, monoanions and dianions of fluorinated copper (II) phthalocyanines are formed in **1** and **2**, respectively. Geometric parameters of the macrocycles in pristine and reference compounds, and salts **1**-**4** are listed in Table 3.

Parent phthalocyanine macrocycle and its halogenated derivatives have stable aromatic 18 π-electron systems. Addition of one or two electrons under reduction leads to the formation of less stable 19 or 20 π-electron systems, respectively. This is accompanied by partial disruption of phthalocyanine aromaticity. Previously it was shown that the most significant changes are observed for the lengths of the $N_{meso} - C$ bonds [8,10,14,21,22]. There is no alteration of these bonds in pristine $Cu^{II}Pc$ [23] and perfluorinated $Cu^{II}(F_{16}Pc)$ [24] but slight alteration is observed for $Cu^{II}(F_8Pc)$ (Table 3) [5]. The shorter and longer $N_{meso} - C$ bonds appear for the [Cu$^{II}(F_8Pc)^{\bullet 3-}$]$^-$ monoanions (the difference between them is 0.040(4) Å), and this difference increases to 0.091(8) Å in the [Cu$^{II}(F_8Pc)^{4-}$]$^{2-}$ dianions. Alternation occurs in such a way that shorter and longer $N_{meso} - C$ bonds belong to two oppositely located fluoro substituted isoindole units (Fig. 2). Thus, alternation increases with negative charge on the macrocycle. A different situation is observed for perfluorinated $Cu^{II}(F_{16}Pc)$. Alternation of the $N_{meso} - C$ bond lengths in the [Cu$^{II}(F_{16}Pc)^{\bullet 3-}$]$^-$ monoanion is close to that for neutral $CuF_{16}Pc$. It is more pronounced for the [Cu$^{II}(F_{16}Pc)^{4-}$]$^{2-}$ dianions (0.058(3) Å) but alternation is still smaller in comparison with that for [Cu$^{II}(F_8Pc)^{4-}$]$^{2-}$ (0.091(8) Å). This effect can be attributed most probably to higher delocalization of negative electron density of the anions on the electron accepting fluorine atoms instead of π-system of the macrocycle, and as expected it is larger for hexadecafluorophthalocyanine than for octafluorophthalocyanine.

Reduction of $Cu^{II}(F_8Pc)$ is also accompanied by appreciable elongation of the C-F bonds (Table 3) whereas the C-F bond lengths for reduced species of $Cu^{II}(F_{16}Pc)$ in **2** and **4** are rather close to that in pristine $Cu^{II}(F_{16}Pc)$ (Table 3). At the same time both salts show elongation of these bonds as it evidences from IR spectra since the absorption bands attributed to the C-F vibrations are shifted to smaller wavenumbers.

Table 3. Bond lengths in pristine copper(II) macrocycles and their anionic salts.

Compound	Charge state of the macrocycle	Average length of the bonds, Å			
		Cu-N$_{pyr}$	C-N$_{pyr}$ short/long, difference	C-N$_{meso}$ short/long, difference	average C-F
Cu^{II}(Pc)$^{2-}$ [23]	−2	1.951(2)	1.384(2)	1.354(2)/1.354(2) 0	−
(Bu$_4$N$^+$)$_2$[Cu^{II}(Pc)$^{•3-}$]$^-$·Br [14]	−3	1.963(1)	1.387(2)	1.320(2)/1.357(2) 0.037(3)	−
Cu^{II}(F$_8$Pc)$^{2-}$ [5]	−2	1.939(5)	1.375(8)	1.313(8)/1.341(8) 0.028(11)	1.352(7)
{cryptand(Na$^+$)}[Cu^{II}(F$_8$Pc)$^{•3-}$]$^-$ (**1**)	−3	1.954(2)	1.377(3)	1.312(3)/1.352(3) 0.040(4)	1.360(2)
{Bu$_4$N$^+$}$_2$[Cu^{II}(F$_8$Pc)$^{4-}$]$^{2-}$·2C$_6$H$_4$Cl$_2$ (**3**) [15]	−4	1.961(5)	1.364(8)/ 1.456(8) 0.092	1.283(8)/1.374(8) 0.091(8)	1.381(7)
Cu^{II}(F$_{16}$Pc)$^{2-}$ [24]	−2	1.948 (16) 1.956(17)	1.382 (3) 1.373(2)	1.320(3)/1.323(2) 0.003(3)	1.346(2) 1.341(2)
[Cu^{II}(F$_{16}$Pc)$^{•3-}$]$^-$ in (PPN$^+$)$_3$[Cu(F$_{16}$Pc)]$_3$$^{3-}$·2C$_6H_5$CN (**4**) [15]	−3	1.954(2)	1.377(2)	1.326(2)/ 1.326(2) 0	1.345(2)
{cryptand(Na$^+$)}$_2$[Cu^{II}(F$_{16}$Pc)$^{4-}$]$^{2-}$ (**2**)	−4	1.954 (2)	1.383(2)	1.305(2)/1.363(2) 0.058(3)	1.348(2)

The [Cu^{II}(F$_8$Pc)$^{•3-}$]$^-$ monoanions in **1** form closely packed π−stacks arranged along the *a* axis and isolated from each other by the cryptand(Na$^+$) cations (Fig. 3). These stacks are not uniform and the {[Cu^{II}(F$_8$Pc)$^{•3-}$]$^-$}$_2$ π-stacking dimers with shorter interplanar distances can be outlined within the stacks. An interplanar distance between phthalocyanines in these dimers is 3.188 Å whereas such distance between the macrocycles from the neighboring dimers is 3.292 Å. The number of van der Waals C, N…C, N contacts is essentially larger in the dimers than those between the dimers.
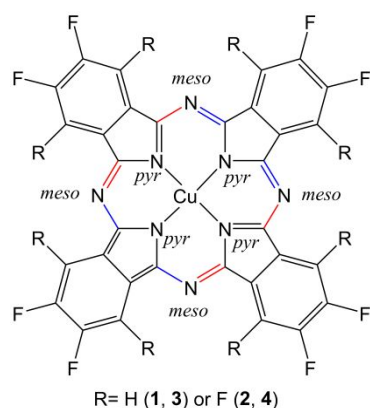
Figure 2. Scheme of fluorinated macrocycle (R = H or F) with elongated and shortened N$_{meso}$ − C bonds (blue and red color, respectively).
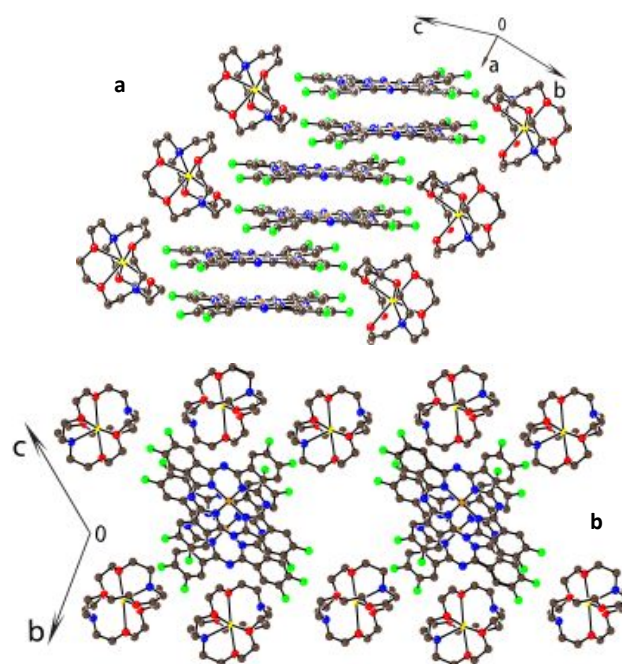
Figure 3. Crystal structure of {cryptand(Na$^+$)}[Cu^{II}(F$_8$Pc$^{•3-}$)]$^-$ (**1**). Views on (a) and along (b) π-stacking columns from the [Cu^{II}(F$_8$Pc$^{•3-}$)]$^-$ radical anions surrounded by cations. Vacancies between the stacks are also occupied by strongly disordered solvent C$_6$H$_4$Cl$_2$ molecules (not shown).

Such interplanar distances are close to those in the stacks of the [Cu^{II}(F$_{16}$Pc)]$^-$ anions in **4** in which trimers with shorter interplanar distance of 3.187 Å are formed whereas such distance between the macrocycles from the neighboring trimers is 3.275 Å [15]. Interplanar distances are also rather longer for the uniform stacks of neutral Cu^{II}(F$_8$Pc) (3.288 Å) [5] and Cu^{II}(F$_{16}$Pc) (3.248 Å) [24]. Formation of closely packed π-stacking dimers in **1** and π-stacking trimers in **4** explains the appearance of broad CT bands in the NIR spectra of these salts (see section with optical spectra).

The [Cu^{II}(F$_8$Pc)$^{•3-}$]$^-$ anions in the π-stacking dimers of **1** (Fig. 4a) are only slightly shifted relative to each other, and Cu^{II} atom of one macrocycle is located above the Cu – N$_{pyr}$ bond of the neighboring macrocycle. That leads to a short intermolecular Cu^{II} ··· Cu^{II} distance of 3.319 Å (Fig. 4a). Macrocycles of the neighboring dimers are shifted essentially stronger relative to each other. As a result, the Cu^{II} atom of one macrocycle is located above the phenylene group of another macrocycle, and the intermolecular Cu^{II} - Cu^{II} distance is 6.646 Å in this case (Fig. 4b).

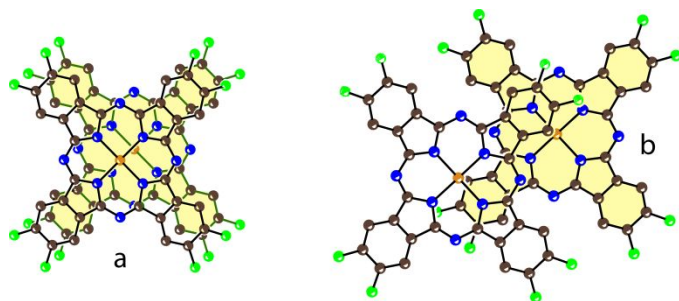**Figure 4.** Types of overlapping mode of the macrocycles in the π-stacks of [Cu^{II}(F$_8$Pc)$^{•3-}$]$^-$. The most distant macrocycle is shown by yellow color and dark green bonds. Hydrogen atoms are omitted.

The [Cu^{II}(F$_{16}$Pc)$^{4-}$]$^{2-}$ dianions form chains along the *a* axis in **2**, each dianion in the chain has 10 short van der Waals (vdW) C, F…C, F contacts of 3.134- 3.484 Å length with two neighboring macrocycles (Fig. 5a). Most probably, close packing of the [Cu^{II}(F$_{16}$Pc)$^{4-}$]$^{2-}$ macrocycles in chains in **2** provides the appearance of an CT band in the NIR spectrum (see above). Chains are isolated by bulky {cryptand(Na$^+$)} cations since the shortest C, F···C, F approach between the macrocycles from the neighboring chains is 3.84 Å (essentially exceed the sum of van der Waals radii) (Fig. 5b). View along four phthalocyanine chains is shown in Fig. 5b. It is seen that there are channels between the chains occupied by {cryptand(Na$^+$)} cations and disordered solvent molecules (not shown in Fig. 5b).
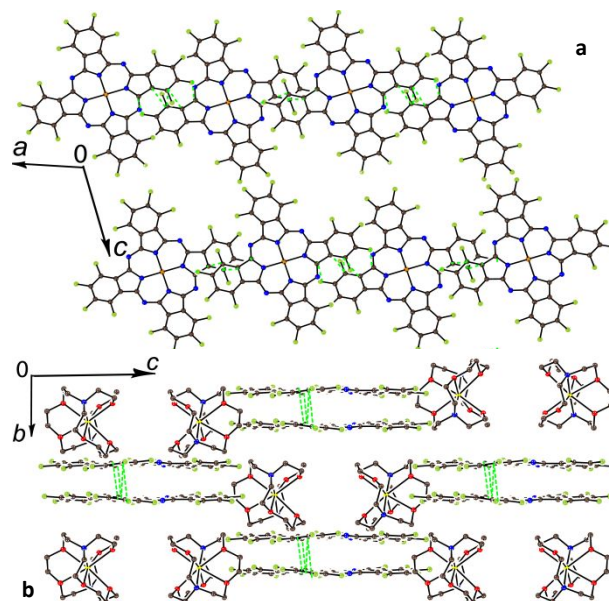

Figure 5. Crystal structure of {cryptand(Na$^+$)}$_2$[Cu^{II}(F$_{16}$Pc)$^{4-}$]$^{2-}$ (**2**). Views on two chains (a) and along four such chains (b) from the [Cu^{II}(F$_{16}$Pc)$^{4-}$]$^{2-}$ dianions surrounded by the cations. Short van der Waals contacts are shown by green dashed lines.

d. Magnetic properties

The magnetic properties of polycrystalline salts were studied by EPR and SQUID techniques. Data of magnetic measurements for the discussed salts are listed in Table 4.

The $\chi_M T$ value for salt **1** is 0.714 emu·K/mol at 300 K (Fig. 6a), which is close to the value of 0.75 emu·K/mol calculated for a system with two non-interacting S = 1/2 spins. These spins are regarded to originate from copper(II) and radical trianion (F$_8$Pc)$^{•3-}$ macrocycle. The Weiss temperatures -9 K (Fig. S3) estimated for **1** indicates moderate antiferromagnetic coupling of spins. The temperature dependence of molar magnetic susceptibility of **1** has maximum at 9 K below which it decreases (Fig. 6b).

Table 4. Magnetic data for **1** - **4** measured by EPR and SQUID techniques.

Compound (spin state)	SQUID			EPR
	Magnetic moment, μ_B	Weiss temperature, K	Magnetic exchange interaction constant, J/k_B, K	
{cryptand(Na$^+$)} [Cu^{II}(F$_8$Pc)$^{\bullet 3-}$]$^-$ (**1**) (*S* = 1/2+1/2)	2.39	- 9	*intra*-dimer $J_{Rad-Rad}$ = − 21.8 cm^{-1} *inter*-dimer $J_{Rad-Rad}$ = − 14.6 cm^{-1} J_{Cu-Rad} = − 10.8 cm^{-1} J_{Cu-Cu} = − 1.5 cm^{-1} Maximum on temperature dependence of magnetic susceptibility at 9 K	Intermediate signal of Cu^{II} and (F$_8$Pc)$^{\bullet 3-}$ (*g* = 2.1652 (*ΔH*=95.02 mT) at RT) The hyperfine interaction of the unpaired electron on Cu^{II} atoms with the nuclear spin of ^{63}Cu and ^{65}Cu (*I* = 3/2) below 155 K
{Bu$_4$N$^+$}$_2$ [Cu^{II}(F$_8$Pc)$^{4-}$]$^{2-}$·2C$_6$H$_4$Cl$_2$ (**3**) [15] (*S* = 1/2)	1.60	- 4	–	The hyperfine interaction of the unpaired electron on Cu^{II} atoms with the nuclear spin of ^{63}Cu and ^{65}Cu (*I* = 3/2) ($g_{||}$=2.0971 (A$_{||}$=26.56 mT), $g_\perp$= 1.9628 at RT)
(PPN$^+$)$_3$[Cu(F$_{16}$Pc)]$_3$$^{3-}$ ·2C$_6$H$_5$CN (**4**) containing dimers from paramagnetic [Cu^{II}(F$_{16}$Pc)$^{\bullet 3-}$]$^-$ isolated by diamagnetic [Cu^{I}(F$_{16}$Pc)$^{2-}$]$^-$ [15] (*S* = 1/2+1/2+1/2+1/2 per formula unit)	3.25	-21.5	J_{inter}/k_B = - 23.5 K (intermolecular interaction between (F$_{16}$Pc)$^{\bullet 3-}$ units) J_{intra}/k_B =- 8.1 K (intramolecular interaction between Cu^{II} and (F$_{16}$Pc)$^{\bullet 3-}$	Not observed
{cryptand(Na$^+$)}$_2$ [Cu^{II}(F$_{16}$Pc)$^{4-}$]$^{2-}$ (**2**) (*S* = 1/2)	1.95	- 1	–	The hyperfine interaction of the unpaired electron on Cu^{II} atoms with the nuclear spin of ^{63}Cu and ^{65}Cu (*I* = 3/2) ($g_{||}$=2.1806 (A$_{||}$=20.11 mT), $g_{\perp}$= 1.9597 at RT) ($g_{||}$=2.1638 (A$_{||}$=21.66 mT), $g_{\perp}$= 1.9586 at 4.2 K)

As described in the crystal structure section the [Cu^{II}(F$_8$Pc)$^{\bullet 3-}$]$^-$ anions are packed in the stacks within which the {[Cu^{II}(F$_8$Pc)$^{\bullet 3-}$]$^-$}$_2$ dimers with shorter interplanar distances can be outlines. Magnetic behavior of salt **1** was modeled using PHI[25], presented by Chilton *et al.*, a software package for modelling complex molecular structures incorporating single or many magnetic centers. Using the built-in UI of PHI, the system could be described by means of an isotropic spin Hamiltonian and treated in terms of *intra*-dimer and *inter*-dimer interactions, with the dominant one being observed between radical trianion (F$_8$Pc)$^{\bullet 3-}$ species of two phthalocyanine [Cu^{II}(F$_8$Pc)$^{\bullet 3-}$]$^-$ subunits in the dimers ($J_{Rad-Rad}$). Additionally, copper(II)-radical (J_{Cu-Rad}) and minor copper(II)-copper(II) (J_{Cu-Cu}) exchanges were taken into account, and the radical-radical interaction between the two pairs of dimers is also observed (*inter*-dimer $J_{Rad-Rad}$). Rather good fitting (Fig. 6a, red curve, R = 0.9963) with four coupling constants yielded $J_{Rad-Rad}$ = − 21.8 cm^{-1}, J_{Cu-Rad} = − 10.8 cm^{-1}, *inter*-dimer $J_{Rad-Rad}$ = − 14.6 cm^{-1} and small but non-negligible J_{Cu-Cu}= − 1.5 cm^{-1}; as well as g^{Cu} = 2.093 for d^9 center while g^{Rad} was fixed at 2. The values indicate a significant degree of AF interactions within the system both between the radical trianion macrocycle species in the dimers and also between the dimers. Weaker interactions involve paramagnetic Cu(II) centers (those are intramolecular Cu(II) interaction with the radical trianion macrocycles and between the nearest Cu(II) centers).
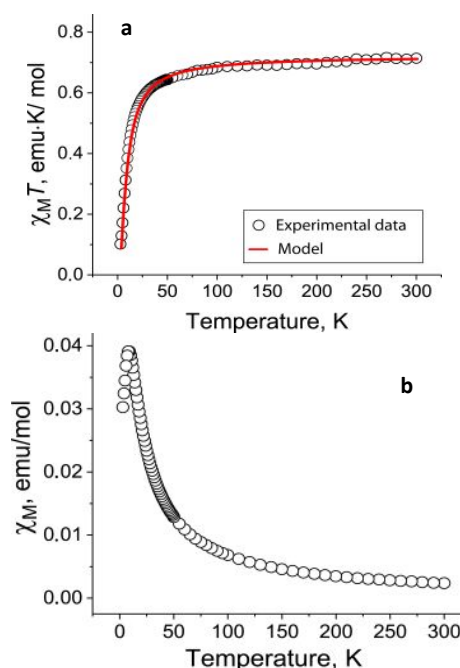
Figure 6. Temperature dependence of $\chi_M T$ value (a) and molar magnetic susceptibility (b) for salt **1**. Fitting of the $\chi_M T$ data using PHI program is shown by red curve.

Such magnetic behavior agrees well with the crystal structure of salt **1** containing dimers with a short interplanar distance between two [Cu^{II}(F$_8$Pc)$^{\bullet 3-}$]$^-$ species. The Cu^{II}···Cu^{II} distance in these dimers is slightly longer, while macrocycles from the neighboring dimers interact essentially weaker with a longer Cu^{II}···Cu^{II} distance. That

allows one to use 4J model as shown above. Previously, it was even found that magnetic interactions between paramagnetic central metal atoms and radical trianion Pc$^{•3-}$ macrocycles are generally weak in the isolated [M(Pc)$^{•3-}$]$^-$ units (M = Cu^{II}, V^{IV}O) (Weiss temperature is only - 2 − - 4 K) [10,15]. A similar situation is observed for oxidized CuPc (in this case Weiss temperature is only - 4.2 K) [26]. At the same time the formation of π-stacking dimers generally provides essentially stronger intermolecular coupling between Pc$^{•3-}$ spins in comparison with the intramolecular V^{IV}O and Pc$^{•3-}$ interactions. For example, such behavior is demonstrated by many systems based on {V^{IV}O(Pc)$^{•3-}$]$^-$ [7]. The value of effective magnetic moment of salt **4** with [Cu^{II}(F$_{16}$Pc)$^{•3-}$]$^-$ is 3.25 μ$_B$ at 300 K
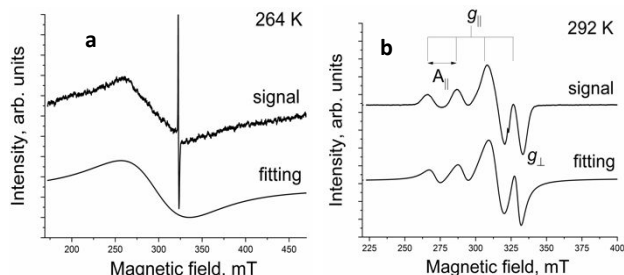

Figure 7. EPR spectra of polycrystalline salts **1** (a) and **2** (b) at 264 K and 292 K, respectively.

with dominant intermolecular coupling between the (F$_x$Pc)$^{•3-}$ radical trianions. The intramolecular Cu^{II} and (F$_x$Pc)$^{•3-}$ coupling for fluorinated copper(II) phthalocyanines is essentially stronger than that observed for monoanions of unsubstituted copper(II) phthalocyanines.

EPR spectrum of **1** (Fig. 7a, S4, S5) contains a broad signal with g = 2.1652 (ΔH = 95.02 mT) at room temperature. Such g- factor is intermediate between those for the Cu^{II} and Pc$^{•3-}$ species in [Cu^{II}(Pc$^{•3-}$)]$^-$ [14]. Therefore, this signal can appear from both paramagnetic species having strong exchange interactions. This broad signal strongly narrows with the temperature decrease (Fig. S5). Additionally to the main broad line, EPR spectrum contains a narrow line with g-factor close to 2.0000 (Fig. 7a) but integral intensity of this line is less than 0.1 % from intensity of the broad line. In addition, the hyperfine splitting at the interaction of unpaired electrons with nuclear spins of ^{63}Cu and ^{65}Cu (I = 3/2) is manifested in the EPR spectrum of **1** below 155 K.

The $\chi_M T$ value for salt **2** is 0.478 emu·K/mol at 300 K corresponding to the contribution of about one non-interacting S = 1/2 spin attributed to Cu^{II}, whereas the (F$_{16}$Pc)$^{4-}$ tetraanions are diamagnetic. Previously it was also found that tetraanion Pc^{4-} [20] and free-base tetrapyrazinoporphyrazine (H$_2$TPyzPz)$^{2-}$ [8,21,22] and naphthalocyanine (H$_2$Nc)$^{2-}$ [27] dianions are also diamagnetic. Only weak antiferromagnetic coupling of spins with Weiss temperatures up to − 1 K is observed in **2** (Fig. S6b). It can be explained by long distances (more than 11 Å) between the paramagnetic Cu^{II} centers within the phthalocyanine chains. Similar behavior with small Weiss temperature of -4 K was shown in previously studied salt **3** with[Cu^{II}(F$_8$Pc^{4-})]$^{2-}$ since in this case isolated arrangement of these dianions also provides long distances between the paramagnetic Cu^{II} centers [15].

corresponding to the contribution of four non-interacting S = 1/2 spins per formula unit. Spins were assigned to the [Cu^{II}(F$_{16}$Pc)$^{•3-}$]$^-$ species which form dimers separated by diamagnetic [Cu^I(F$_{16}$Pc)$^{4-}$]$^-$ anions. Probing of magnetic behavior of **4** by four spin model[15] also shows stronger intermolecular (J/k_B= - 23.5 K) and weaker

intramolecular coupling (J/k_B = - 8.1 K). It should be noted that these values are very close to the $J_{Rad-Rad}$ and J_{Cu-Rad} values obtained for **1**. The *inter*-dimer $J_{Rad-Rad}$ value is zero for **4** since dimers are separated by diamagnetic [Cu^I(F$_{16}$Pc)$^{4-}$]$^-$ anions. Thus, pair arrangement of the [Cu^{II}(F$_x$Pc)$^{•3-}$]$^-$ species in **1** and **4** provides similar magnetic behavior

A strongly asymmetric signal in the EPR spectrum of **2** with $g_{||}$ = 2.0971 - 2.1806 ($A_{||}$ = 20.11 - 26.56 mT) and $g_\perp$ = 1.9597 - 1.9628 can be attributed to Cu^{II} (Table 4, Fig. 7b, S7). Such parameters are characteristic of tetragonal Cu(II) complexes with four nitrogen atoms in the equatorial coordination of a Cu^{II} shell [28]. The hyperfine interactions of the unpaired electron of Cu^{II} with the ^{63}Cu and ^{65}Cu (I = 3/2) nuclear spins are also observed where the signal associated with $g_\perp$ overlaps with those of $g_{||}$ and only three of the four lines associated with $g_{||}$ can be distinguished. The fine structure caused by hyperfine coupling of Cu^{II} spin with nitrogens atoms is not observed in the spectrum of **2**. EPR spectra of **2** remain almost unchanged upon cooling down to 4 K (Fig. S7, Table 4). Similar behavior is observed for salt **3** with [Cu^{II}(F$_8$Pc)$^{4-}$]$^{2-}$ in which spin is also localized exclusively on the Cu^{II} atoms (Table 4).

Thus, formation of salts **1** - **4** is accompanied by one- or two-electron reduction of the macrocycles. One electron reduction leads to [Cu^{II}(F$_x$Pc)$^{•3-}$]$^-$ anions with two S = 1/2 spins positioned on Cu^{II} and (F$_x$Pc)$^{•3-}$. Two-electron reduction up to the [Cu^{II}(F$_x$Pc)$^{4-}$]$^{2-}$ dianions yields only one S = 1/2 spin localized exclusively on the Cu^{II} atoms and showing HF interactions. The (F$_x$Pc)$^{4-}$ tetraanions are diamagnetic and EPR silent.

Conclusion

New salts based on reduced copper(II) octafluoro- and hexadexafluorophthalocyanines were obtained and characterized. Combined with the previously obtained results, this work revealed the features of [Cu^{II}(F$_x$Pc)]$^{n-}$ (x = 8, 16, n = 0, 1, 2). Reduction is accompanied by blue shift of the Q-band and the appearance of new weak bands in the NIR range. Partial disruption of macrocycle aromaticity is pronounced in the alternation of the N$_{meso}$-C bonds within the macrocycles. In case of Cu^{II}(F$_8$Pc) this effect is more pronounced for the dianions but perfluorinated Cu^{II}(F$_{16}$Pc)$^{n-}$ (n = 1, 2) anions generally show weaker alternation of the bonds in comparison with Cu^{II}(F$_8$Pc). It is shown that two S = 1/2 spins are positioned on Cu^{II} and (F$_x$Pc)$^{•3-}$ of [Cu^{II}(F$_x$Pc)$^{•3-}$]$^-$. In the columnar stack of dimerized [Cu^{II}(F$_x$Pc)$^{•3-}$]$^-$, stronger intermolecular coupling between (F$_x$Pc)$^{•3-}$ and slightly weaker intramolecular interaction are observed between Cu^{II} and (F$_x$Pc)$^{•3-}$. This work showed that coupling between central metal atom and paramagnetic macrocycle is rather strong for fluorinated copper(II) phthalocyanines and is essentially stronger than that observed for reduced unsubstituted copper(II) phthalocyanines. Upon two-electron reduction, the [Cu^{II}(F$_x$Pc)$^{4-}$]$^{2-}$ dianions are formed with one S = 1/2 spin localized

exclusively on Cu^{II}. Only weak magnetic coupling of spins is observed in this case. Large macrocycles are packed in the π-stacks. However, dimerization of the macrocycles within the stacks or metal to the macrocycle charge transfer still prevent the observation of high conductivity in them, and only magnetic coupling is observed within the dimers. The size and shape of the cations can affect dimerization within the stacks and we plan to study the salts of such type with the cations of different size and shape. This work is now in progress.

Experimental

Materials

Copper (II) octafluorophthalocyanine $[Cu^{II}(F_8Pc)]$ and copper (II) hexadecafluorophthalocyanine $[Cu^{II}(F_{16}Pc)]$ (>98% purity, sublimation grade) were purchased from TCI. 4,7,13,16,21,24-Hexaoxa-1,10-diazabicyclo[8.8.8]hexacosane (cryptand[2.2.2], Acros, 98%) and dicarbonylcyclopentadienyl cobalt (I) (CpCo(CO)$_2$, Sigma-Aldrich, technical grade) were used as received. Reductant $(Na^+)[CpCo(CO)_2^-]$ was obtained as described [29]. Solvents were purified in argon atmosphere. o-Dichlorobenzene ($C_6H_4Cl_2$) was distilled over CaH_2 under reduced pressure; n-hexane was distilled over Na/benzophenone. The solvents were degassed and stored in a glove box which contained less than 1ppm of water and oxygen. The crystals of **1** and **2** were isolated and stored in the glove box. KBr pellets for IR- and UV-visible-NIR measurements were also prepared in the glove box. EPR measurements and SQUID measurements for **1** and **2** were performed on polycrystalline samples sealed in 2 mm quarz tubes under ambient pressere of argon gas.

Syntheses of crystalline salts 1-2

The crystals of **1**-**2** were obtained by diffusion technique. The final solution was cooled down to room temperature and filtered into in a 50 mL glass tube of 1.8 cm diameter with a ground glass plug. 30 mL of n-hexane was layered over the solution. Slow mixing of two solvents during 1 month provided precipitation of crystals on the walls of the tube. The solvent was decanted from the crystals and they were washed with n-hexane.

{Cryptand(Na$^+$)}[Cu^{II}(F$_8$Pc)$^{•3-}$]$^-$ ·2C$_6$H$_4$Cl$_2$ (**1**) was obtained via the reduction of Cu^{II}(F$_8$Pc) (30 mg, 0.042 mmol) with an excess of NaCpCo(CO)$_2$ (20 mg, 0.099 mmol) in the presence of two equivalents of cryptand[2.2.2] (32 mg, 0.084 mmol) in 16 ml of o-dichlorobenzene. The reaction was performed for one day at 80°C. The resulting deep blue-violet solution was cooled down to room temperature and filtered into a tube for crystal growth. Dark black blocks with metallic luster were obtained in 54% yield.

{Cryptand(Na$^+$)}$_2$[Cu^{II}(F$_{16}$Pc)$^{4-}$]$^{2-}$ ·C$_6$H$_{14}$ (**2**) was obtained via the reduction of Cu^{II}(F$_{16}$Pc) (36 mg, 0.042 mmol) with an excess of NaCpCo(CO)$_2$ (20 mg, 0.099 mmol) in the presence of two equivalents of cryptand[2.2.2] (32 mg, 0.084 mmol) in 16 ml of o-dichlorobenzene. The reaction was performed for one day at 80°C. The resulting deep violet solution was cooled down to room temperature and filtered into a tube for crystal growth. Dark black block with metallic luster were obtained in 61% yield.

The composition of **1** and **2** (Table 1) was determined from X-ray diffraction on single crystals. The analysis of the obtained

crystals under microscope in a glove box as well as testing of several single crystals from each synthesis by X-ray diffraction showed that only one crystalline phase is formed. Elemental analysis cannot be used to support the composition of the obtained crystals due to their air sensitivity.

General

UV-visible-NIR spectra were measured in KBr pellets on a PerkinElmer Lambda 1050 spectrometer in the 250-2500 nm range. FT-IR spectra were obtained in KBr pellets with a PerkinElmer Spectrum 400 spectrometer (400-7800 cm^{-1}). EPR spectra were recorded on polycrystalline samples of **1** and **2** with a JEOL JES-TE 200 X-band ESR spectrometer equipped with a JEOL ES-CT470 cryostat. A Quantum Design MPMS-XL SQUID magnetometer was used to measure static magnetic susceptibility of **1** and **2** at 1 kOe magnetic field in cooling and heating conditions in the 300 - 1.9 K range. The sample holder contribution and core temperature independent diamagnetic susceptibility (χ_d) were subtracted from the experimental values. The χ_d values were estimated from the extrapolation of the data in the high-temperature range by fitting the data with the following expression: $\chi_M = C/(T - \Theta) + \chi_d$, where C is the Curie constant and Θ is Weiss temperature. Effective magnetic moments (μ_{eff}) were calculated with the formula: $\mu_{eff} = (8\chi_M T)^{1/2}$.

Crystal structure determination

Crystallographic data for **1** and **2** are listed in Table 5. The data for **1** and **2** were collected on an Oxford diffraction "Gemini-R" CCD diffractometer with graphite monochromated MoK$_\alpha$ radiation using an Oxford Instrument Cryojet system. Raw data reduction to F^2 was carried out using CrysAlisPro, Oxford Diffraction Ltd [30]. The structures were solved by direct method and refined by the full-matrix least-squares method against F^2 using SHELX 2016 [31] and Olex2 [32]. Non-hydrogen atoms were refined in the anisotropic approximation. Positions of hydrogen were calculated geometrically.

Table 5. X-ray diffraction data for **1** and **2**

| Compound	1	2
Emp. formula	$C_{50}H_8CuF_8N_{10}NaO_6$	$C_{68}H_{72}CuF_{16}N_{12}Na_2O_{12}$
	(+ squeezed $2C_6H_4Cl_2$	(+ squeezed C_6H_{14}
	molecules)	molecule)
M_r [g·mol^{-1}]	1083.19	1662.89
Color and shape	metallic dark black block	metallic dark black block
Crystal system	triclinic	monoclinic
Space group	$P\bar{1}$	$I\,2/a$
a, Å	8.5781(3)	22.0273(5)
b, Å	18.3416(5)	11.7156(2)
c, Å	19.5860(6)	30.5920(7)
α, °	117.097(3)	90
β, °	91.796(2)	108.615(2)
γ, °	103.120(3)	90
V, Å^3	2639.27(16)	7481.7(3)
Z	2	4
ρ_{calc} [g/cm^3]	1.363	1.476
μ [mm^{-1}]	0.506	0.411
F(000)	1076	3420
T [K]	118(2)	117.6(9)
Max. 2Θ, °	59.514	56.564
Reflns measured	46612	39700
Unique reflns	13152	8928
Parameters	815	501
Restraints	468	0
Reflns[$F_o>2(F_o)$]	10718	6584
R_1 [$F_o>2\sigma(F_o)$]	0.0462	0.0516
WR_2 (all data)^a,	0.1209	0.1355
G.O.F	1.020	1.022
CCDC number	1986506	1986508

Acknowledgements

Notes and references

1 R. Zeis, T. Siegrist and Ch. Kloc, *Appl. Phys. Lett.*, 2005, **86**, 022103.
2 Z. Bao, A. J. Lovinger and J. Brown, *J. Am. Chem. Soc.*, 1998, **120**, 207–208.
3 R. W. I. de Boer, A. F. Stassen, M. F. Craciun, C. L. Mulder, A. Molinari, S. Rogge and A. F. Morpurgo, *Appl. Phys. Lett.*, 2005, **86**, 262109.
4 H. Jiang, P. Hu, J. Ye, Y. Li, H. Li, X. Zhang, R. Li, H. Dong, W. Hu and C. Kloc, *Adv. Mater.*, 2017, **29**, 1605053.
5 A. Matumoto, N. Hoshino, T. Akutagawa and M. Matsuda, *Applied Sciences*, 2017, **7**, 1111.
6 H. Jiang, J. Ye, P. Hu, F. Wei, K. Du, N. Wang, T. Ba, S. Feng and C. Kloc, *Sci Rep*, 2015, **4**, 7573.
7 D. V. Konarev, A. V. Kuzmin, S. S. Khasanov, M. S. Batov, A. Otsuka, H. Yamochi, H. Kitagawa and R. N. Lyubovskaya, *CrystEngComm*, 2018, **20**, 385–401.

8 M. A. Faraonov, D. V. Konarev, A. M. Fatalov, S. S. Khasanov, S. I. Troyanov and R. N. Lyubovskaya, *Dalton Trans.*, 2017, **46**, 3547–3555.
9 D. V. Konarev, M. A. Faraonov, A. V. Kuzmin, S. S. Khasanov, Y. Nakano, S. I. Norko, M. S. Batov, A. Otsuka, H. Yamochi, G. Saito and R. N. Lyubovskaya, *New J. Chem.*, 2017, **41**, 6866–6874.
10 D. V. Konarev, M. A. Faraonov, A. V. Kuzmin, N. G. Osipov, S. S. Khasanov, A. Otsuka, H. Yamochi, H. Kitagawa and R. N. Lyubovskaya, *New J. Chem.*, 2019, **43**, 19214–19222.
11 D. E. C. Yu, M. Matsuda, H. Tajima, A. Kikuchi, T. Taketsugu, N. Hanasaki, T. Naito and T. Inabe, *J. Mater. Chem.*, 2009, **19**, 718–723.
12 T. H. Q. Nguyen, M. Pelmuş, C. Colomier, S. M. Gorun and D. Schlettwein, *Phys. Chem. Chem. Phys.*, 2020, **22**, 7699–7709.
13 A. B. P. Lever, E. R. Milaeva and G. Speier, *Phthalocyanines: Properties and Applications*, New York, VCH Publishers., 1993, vol. 3.
14 D. V. Konarev, A. V. Kuzmin, M. A. Faraonov, M. Ishikawa, S. S. Khasanov, Y. Nakano, A. Otsuka, H. Yamochi, G. Saito and R. N. Lyubovskaya, *Chem. Eur. J.*, 2015, **21**, 1014–1028.
15 D. V. Konarev, S. I. Troyanov, A. V. Kuzmin, Y. Nakano, M. Ishikawa, M. A. Faraonov, S. S. Khasanov, A. L. Litvinov, A. Otsuka, H. Yamochi, G. Saito and R. N. Lyubovskaya, *Inorg. Chem.*, 2017, **56**, 1804–1813.
16 D. V. Konarev, A. V. Kuzmin, M. Ishikawa, Y. Nakano, M. A. Faraonov, S. S. Khasanov, A. Otsuka, H. Yamochi, G. Saito and R. N. Lyubovskaya, *Eur. J. Inorg. Chem.*, 2014, **2014**, 3863–3870.
17 D. V. Konarev, L. V. Zorina, M. Ishikawa, S. S. Khasanov, A. Otsuka, H. Yamochi, G. Saito and R. N. Lyubovskaya, *Crystal Growth & Design*, 2013, **13**, 4930–4939.
18 R. O. Loutfy, C. K. Hsiao, B. S. Ong and B. Keoshkerian, *Can. J. Chem.*, 1984, **62**, 1877–1885.
19 Ayman Nafady, Ali M. Alsalme, Khalid. A. AL-Farhan, Rafat M. El Khatib, Suresh Bhargava, *Int. J. Electrochem. Sci.*, 2014, **9**, 8131–8144.
20 D. V. Konarev, A. V. Kuzmin, S. S. Khasanov, A. L. Litvinov, A. Otsuka, H. Yamochi, H. Kitagawa and R. N. Lyubovskaya, *Chem. Asian J.*, 2018, **13**, 1552–1560.
21 M. A. Faraonov, N. R. Romanenko, A. V. Kuzmin, D. V. Konarev, A. F. Shestakov, P. A. Stuzhin, S. S. Khasanov, A. Otsuka, H. Yamochi, H. Kitagawa and R. N. Lyubovskaya, *European Journal of Inorganic Chemistry*, 2019, **2019**, 2918–2923.
22 M. A. Faraonov, N. R. Romanenko, A. V. Kuzmin, D. V. Konarev, S. S. Khasanov and R. N. Lyubovskaya, *Dyes and Pigments*, 2020, **180**, 108429.
23 A. Hoshino, Y. Takenaka and H. Miyaji, *Acta Crystallogr B Struct Sci*, 2003, **59**, 393–403.
24 S. M. Yoon, H. J. Song, I.-C. Hwang, K. S. Kim and H. C. Choi, *Chem. Commun.*, 2010, **46**, 231–233.
25 N. F. Chilton, R. P. Anderson, L. D. Turner, A. Soncini and K. S. Murray, *J. Comput. Chem.*, 2013, **34**, 1164–1175. PHI can be downloaded from the link: http://nfchilton.com/phi.html.
26 T. Inabe and H. Tajima, *Chem. Rev.*, 2004, **104**, 5503–5533.
27 D. V. Konarev, S. S. Khasanov, Y. Nakano, A. F. Shestakov, M. Ishikawa, A. Otsuka, H. Yamochi, H. Kitagawa and R. N. Lyubovskaya, *Eur. J. Org. Chem.*, 2018, **2018**, 3410–3415.
28 L. Quintanar and L. Rivillas-Acevedo, in *Protein-Ligand Interactions*, eds. M. A. Williams and T. Daviter, Humana Press, Totowa, NJ, 2013, vol. 1008, pp. 267–297.
29 D. V. Konarev, A. V. Kuzmin, M. G. Andronov, S. S. Khasanov, M. S. Batov, A. Otsuka, H. Yamochi, H. Kitagawa and R. N. Lyubovskaya, *Inorganica Chimica Acta*, 2018, **483**, 504–509.

30 *Crysalis Bruker AXS Inc.: Madison, Wisconsin*, .
31 G. M. Sheldrick, *Acta Crystallogr A Found Crystallogr*, 2008, **64**,
    112–122.
32 O. V. Dolomanov, L. J. Bourhis, R. J. Gildea, J. A. K. Howard and
    H. Puschmann, *J Appl Crystallogr*, 2009, **42**, 339–341.

Graphical abstract
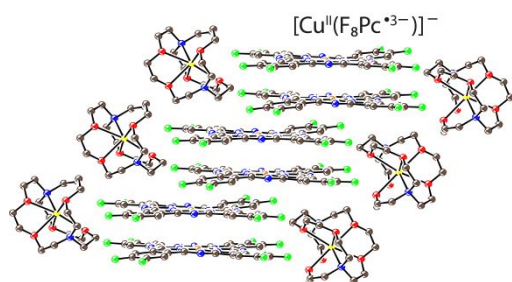
$$[Cu^{II}(F_8Pc^{\bullet 3-})]^-$$

New salts based on reduced copper(II) octafluoro- and hexadexafluorophthalocyanines were obtained and characterized. The effect of reduction on the molecular structure, optical and magnetic properties of the $[Cu^{II}(F_xPc)]^{n-}$ (x = 8 and 16) phthalocyanines in the reduction states (n = 1 and 2) was studied.